Flare-up in Cordilleran arcs controlled by fluxes in subduction water budgets

Timothy Chapman[a]*, Luke A. Milan[a], Sabin Zahirovic[b], Andrew S. Merdith[c], Geoffrey L. Clarke[b], Mingdao Sun[d], Nathan R. Daczko[e]

[a]Earth Science, School of Environmental and Rural Science, University of New England; NSW, 2351, Australia
[b]School of Geosciences, The University of Sydney; NSW, 2006, Australia
[c]School of Earth and Environment, University of Leeds; Woodhouse, Leeds LS2 9JT, UK
[d]State Key Laboratory of Isotope Geochemistry, Guangzhou Institute of Geochemistry, Chinese Academy of Sciences; Guangzhou 510640, China
[e]Department of Earth and Environmental Sciences, Macquarie University; NSW, 2109, Australia

*Corresponding author. Email: timothy.chapman@une.edu.au

Abstract

The tempo of subduction-related magmatic activity over geological time is episodic. Despite intense study and their importance in crustal addition, the fundamental driver of these episodes remains unclear. We demonstrate quantitatively a first order relationship between arc magmatic activity and subduction flux. The volume of oceanic lithosphere entering the mantle is the key parameter that regulates the proportion of H_2O entering the sub-arc. New estimates of subduction zone H_2O budgets over the last 150 million-years indicate a three- to five-fold increase in the proportion of H_2O entering the sub-arc during the most recent global pulse of magmatism. Step changes in H_2O flux enable proportionally greater partial melting in the sub-arc. Similar magmatic pulses in the ancient Earth could be related to variability in subduction flux associated with supercontinent cycles.

Keywords: magmatic flare-ups, magma flux, Continental arc, Earth's tempo, global water budgets, phase equilibria

Plain language summary

Volcanic activity over geological time is episodic. Typical background rates of activity are punctuated by pulses involving 100–1000 times the volume of magma in volcanic arcs. Despite intense study, the main agent that controls this episodic behaviour remains unknown. We demonstrate quantitatively a first order relationship between magmatic activity and the volume of material being subducted. The volume of oceanic lithosphere entering the mantle is the key parameter that regulates the proportion of H_2O budgets. New estimates of subduction zone H_2O budgets over the last 150 million-years indicate a three- to five-fold increase in the proportion of H_2O entering the volcanic arcs. The timing corresponds to the most recent global pulse of magmatism. Step changes in H_2O flux enable proportionally greater partial melting and therefore more magma generation in the crust.

1. Introduction

Subduction zones are key locations for the net growth of continents and the long-term cycling of elements through the crust, mantle, and exosphere (Hawkesworth & Kemp, 2006; Till et al., 2021). The tectonic process of subduction has been inferred to be continuous around the globe for at least the last 2–3 billion years (Hawkesworth & Kemp, 2006; Campbell & Allen, 2008; Voice et al., 2011; Palin & Santosh, 2021). Records of magmatic activity along the margin of continents, based on U–Pb crystallization ages from zircon, should present as a broad continuum associated with ongoing subduction. However, the preserved geological record is marked by peaks of zircon crystallization ages that indicate changing tempos in magmatic activity, whereby lower background rates of magmatism are punctuated by episodic pulses (Fig. 1) (Cagnioncle et al., 2007; Campbell & Allen, 2008; Voice et al., 2011; Chapman et al., 2021). Aspects of the older geological record could reflect a preservation bias, though the pattern is also retained by Phanerozoic aged subduction zone settings (McKenzie et al., 2016; Cao et al., 2017).

The drivers of Phanerozoic episodes of magmatic flare-up remain contentious (see Chapman et al. 2021). This is despite higher resolution geological records of magmatic activity and tectonic parameters for the Phanerozoic subduction zones, compared to those of the Precambrian (Campbell & Allen, 2008; McKenzie et al., 2016; Palin & Santosh, 2021). The causes of episodic magmatic activity are generally ascribed to variations of heat-flux in one part of the subduction system: (1) changes in cycles of compression or extension in the crust (DeCelles et al., 2009; Chapman et al., 2021); or (2) changes in the mantle heat-flux, related to the behaviour of the down-going slab or melting in the mantle wedge (Cagnioncle et al., 2007; Martínez Adrila et al., 2019; Till et al., 2021). Simultaneous increases in magmatic activity along disparate arcs across the globe indicates a fundamental change in mantle heat-flux associated to plate tectonics (Fig. 2). The principal control on mantle

66 melting in subduction zones is the fluid and/or melt capacity of the downgoing slab
67 (Ringwood, 1974; Grove et al., 2006). Deep-time estimates of the H_2O capacity of global
68 subduction zones are determined here based on full-plate reconstructions (Müller et al., 2016)
69 and phase equilibria modelling. The first prediction of long-term variability in H_2O-budgets
70 is correlated to both global and regional magmatic arc activity supporting a first-order
71 tectonic control.

72 **2. Methods**

73 *2.1. Global plate reconstructions*

74 Parameters for global subduction zones and three specific arc segments (New Zealand,
75 Antarctica–Patagonia, East Asia) were extracted using the open-source and cross-platform
76 GPlates software (www.gplates.org) (Müller et al., 2016). Subduction zone kinematics
77 encompassing the subducting plate area, age, thickness as well as obliquities and
78 convergence rates were collated at 1 Myr intervals from the global plate reconstruction (Figs
79 1 & 2). The slab flux was determined as the product of segmented arc length, lithospheric
80 thickness, and orthogonal convergence rate, summed for all subduction zone segments (Fig.
81 1) (East et al., 2019).

82 The modelled seafloor ages in the plate reconstructions are based on seafloor
83 spreading isochrons from *c.* 230 Ma (Fig. 2: East et al., 2019). The spreading rates generate
84 predictions of subduction convergence in a globally consistent model. The subducting plate
85 thickness is calculated based on the cooling of at maximum a 125 km thick lithosphere, with
86 a basal mantle potential temperature of 1350˚C (Grose et al., 2012). The crustal thickness
87 includes oceanic basement and sediment. Sediment thickness estimates are based on model
88 predictions after Zahirovic et al. (2022). Animations of the subduction zone convergence,
89 lithospheric age and sediment thickness are presented in the supplement (S1 & S2).

Restricted preservation of ancient seafloor presents the biggest limitations in the plate reconstruction further back in geological time. The Pacific Plate motion is connected through a plate circuit from 83 to 0 Ma, but for earlier times it moves independently, and the motion is less well constrained. Seafloor ages become less well constrained before 150 Ma as only a small portion of the Pacific Plate triangle is preserved. The plate motions between ~120 and 83 Ma during the Cretaceous Normal Superchron are interpolated as there are no magnetic polarity reversals in this timeframe.

2.2. Seafloor hydration

Initial budgets of H_2O in the oceanic crust and lithosphere were calculated based on global plate reconstructions to *c.* 230 Ma (Fig. 3). The model estimates assume that the proportion of fluid-saturated basaltic crust and extent of serpentinisation varies in relation to mid-ocean ridge spreading rate based on time-dependent calculations of Merdith et al. (2019). Sediment was assumed to be fluid saturated. The models generate a proportion of saturation of oceanic lithosphere that is equivalent to previous estimates (van Keken et al., 2011; Faccenda, 2014).

Uncertainty on the estimates is cumulative in relation to error on spreading rates, lithosphere thicknesses and predicted extent of hydration. Conditional probability was determined based on the range of spreading rates to account for uncertainty on these values (Merdith et al., 2019). A second stage of seafloor hydration associated to trench flexure is poorly constrained but assumed to accounting for an additional 0–2% hydration of the top 10 km of lithospheric mantle (Hacker, 2008; Faccenda, 2014; Cerpa et al., 2022). The assumption of uniform hydration remains limiting on a global deep-time scale. Trench flexure estimates were capped at 2% in the top 10 km in this work. Uncertainty estimates from modern subduction zones show variation in hydration extent in the same range as those used in the calculations of this work (van Keken et al., 2011; Cerpa et al., 2022).

2.3.Phase equilibria modelling

Phase equilibria modelling was performed using THERMOCALC in the NCKFMASHTO chemical system utilising version 3.47i (Powell & Holland, 1988) and the internally consistent thermodynamic dataset 6.2 (updated 6th February 2012) (Holland & Powell, 2011). The modelled bulk rock compositions are based on a MORB (Chapman & Clarke, 2021), pelagic sediment from ODP site 800 (Plank & Langmuir, 1998), and the KLB-1 lherzolite (Davies et al., 2009) (Fig. S1). The utilisation of pelagic sediment was preferred to GLOSS-type to avoid artefacts in the phase equilibria modelling association to oversaturation of that bulk-composition to calcium carbonate (Coulthard et al., 2020). The modelled redox conditions for the MORB were fixed at $Fe^{3+}/[Fe^{3+}+Fe^{2+}] = 0.15$, the metasediments at 0.05, and the serpentinite at 0.03. Fluid was considered in excess. The relative proportion of free H_2O was determined by setting H_2O at molar proportions that just saturated the low-temperature and high-pressure equilibria (Clarke et al., 2006).

Pressure uncertainties for the assemblage field boundaries are approximately ±0.1 GPa at the 2σ level associated to propagation of thermodynamic uncertainties (Powell & Holland, 2008; Chapman et al., 2019). The uncertainties account for ~10% variability in H_2O modes in the calculations, which is within that expected for varying bulk compositions in typical ranges for subducted lithologies (Evans & Bickle, 2006; Palin et al., 2016; Chapman et al., 2019). At high-*P*, sediments would approach the solidus (Hermann & Spandler, 2008), current limitations in phase equilibria models makes assessing the effects of such high-pressure melting difficult (Fig. S1b) (White et al., 2014).

2.4.Subducted H_2O budgets

Utilising modern subduction zone variables and predicted slab thermal histories (Syracuse et al., 2010), H_2O contents across typical *P–T* arrays of modern sub-arcs were calculated based on the phase equilibria (Fig. S1). Average H_2O released based on phase equilibria modelling of slabs from modern systems with fast (>90 km Myr^{-1}), intermediate ($60>x<90$ km Myr^{-1})

and slow (<60 km Myr^{-1}) convergence rates were extracted using two of the end-member thermal models (D80 and W1300) of Syracuse et al. (2010). The H_2O released by MORB for these thermal models in each of the respective bins is as follows: 15.10±1.51, 0.04±0.004 and 0.004±0.0004 Mole %. The H_2O released from pelagic sediment is: 0.047±0.0047, 0.064±0.0064 and 0.068±0.0068 Mole %. The proportions for serpentinite relate to thermal conditions predicted at the Moho of the downgoing lithosphere resulting in the release of the following proportions of H_2O: 31.03±3.1, 31.03±3.10 and 15.77±1.577 Mole %. Uncertainty on these estimates was based on 2 sigma distributions on the estimates of modes from the thermodynamic modelling.

The bins of H_2O release proportions were utilised in the determination of the sub-arc budgets via the integration with subduction kinematic data (Fig. 3). The portion of H_2O entering the sub-arc region was determined based on the slab flux rate, densities of the modelled bulk rocks, normalised to global length of arcs at each million-year time bin. The estimates consider H_2O liberated from structurally bound minerals across typical subduction heating arrays based on predictions from the phase equilibria modelling (Fig. S1).

The method cannot incorporate undetermined physical subduction variables of ancient systems, such as slab dip that also influence sub-arc depth conditions (Syracruse et al., 2010). The time-dependent constraints on the slabs reaching the sub-arc were based therefore on the convergence rates to a nominal depth of 125 km, consistent with most predictions of sub-arc depths (100–150 km). These descent rates are like those established in modern subduction zones (Müller et al., 2016).

Total uncertainty on the subduction zone H_2O budgets was determined using the propagation of error function assuming 2σ level error at each step. The overall uncertainty varies between 30–70% of the calculated values. To assess the validity of the results, the new calculations are compared to previous predictions of H_2O release in modern subduction zones

by van Keken et al. (2011). Integration of these values to subduction flux over time produces similar trends to the results of this work (Fig. 1d). **3. Results**

2.5. Magmatic pulses and lulls

Phanerozoic magmatic activity on the continents has shown regular temporal fluctuation that can be broadly linked to the dispersion or amalgamation of supercontinents (Fig. 1). The most recent pulses in subduction magmatism occurred at *c*. 150–160 Ma and *c*. 100–130 Ma (Fig. 1) (Voice et al., 2011). Similar magmatic peaks are observed at *c*. 250 and 350 Ma (Fig. 1) (McKenzie et al., 2016; Cao et al., 2017; Chapman et al., 2022). Drivers of these magmatic pulses have been variously linked to estimates of the rate of subduction (Fig. 1: Kirsch et al., 2016), its angle of dip (Gorzyk et al., 2007), or the length of subduction segments (Domeier et al., 2018) with mixed results across different arcs. The variability is in part related to uncertainty in the determination of tectonic parameters in local arc segments, like that of western North America (Ducea et al., 2007; Martínez Adrila et al., 2019), associated to sparsely preserved seafloor or the effects of multiple terrane collisions. Furthermore, the rate of subduction presents only one of the important parameters that influence fluid capacity in subduction zones (Fig. 1a).

2.6. Subduction flux

The slab flux at convergent margins is directly related to long-term tectonic cycles (Fig. 1b) (Domeier et al., 2018; East et al., 2019). The breakup of Pangea, beginning in the Triassic, induced faster global average convergence rates at subduction zones and a contemporaneous doubling of mid-ocean ridge lengths (Müller et al., 2016). These dynamics compounded to produce a peak in circum-Pacific subducted slab volume in the Early Cretaceous (*c.* 130 Ma) (Figs 1b & 2). The subsequent slowing of convergence rates and the subduction of younger, thinner slabs along longer subduction zone lengths have contributed to a general decline in slab flux until the present day (East et al., 2019).

The temporal evolution of the subduction flux between 230 Ma and the present day shows a first order correlation with the Cretaceous pulses in global magmatism (Fig. 1b). Evidence for the correlation is preserved in flare-up events identified in *c.* 100–130 Ma segments of Antarctica, North and South America, New Zealand, Antarctica and northern China, Korea, and Japan (Figs 1 & 2) (Kirsch et al., 2016; Cao et al., 2017; Milan et al., 2017; Tang et al., 2018). Predictions of peaks in subduction flux further back in time also show good correlation with pulses in magmatism in the Phanerozoic at *c*. 250 and 350 Ma, associated with the assembly of Pangea and Laurussia (Domeier et al., 2018; Chapman et al., 2022).

Variation in subduction flux is mostly controlled by convergence rates but is enhanced by the thickness of the oceanic crust and the overlying sediment. Unlike oceanic thickness that varies consistently with its age of formation, subducted sediment volume displays more variability over time that can match both high and low magnitude pulses in magmatic activity (Fig. 1d). Periods of thick sediment subduction correlate well with identified episodes of wedge thickening and related metamorphism on arc margins (Fig. 3) (Iwasaki et al., 1995; Gray & Foster, 2004). However, it remains difficult to fully assess the deep burial of sediment due to the uncertainties in the extent of subduction erosion (Clift & Vannucchi, 2004).

2.7. Fluid budgets

The capacity of subducted lithosphere to carry substantial fluid volumes is dependent on the extent of hydration of its differing lithologies and their absolute volumes. The main influential fluid-bearing components are the lithospheric mantle, the MORB-like crust, extent of abyssal serpentinite, and the overlying pelagic sediments. The age of the subducting oceanic crust influences lithospheric thickness, the extent of hydration, and the lithospheric geotherm (van Keken et al., 2011; Schmidt & Poli, 2014; Syracuse et al., 2019). In turn, the

thickness of the sedimentary cover varies not only in relation to seafloor age, but also latitude, and proximity to prominent deltaic systems (Fig. 1c) (Zahirovic et al., 2022). In combination these all control the capacity to carry and release H_2O and other fluids (CO_2, H_2S, SO_2) during subduction.

The location of fluid release from a subducted slab is dependent on the *P–T* path and intersected of multivariant dehydration reactions (Fig. S1) (Clarke et al., 2006; Schmidt & Poli, 2014). The specific depth of the sub-arc region on different margins is primarily dependent on convergence rate as well as slab dip and oceanic crust age (Schmidt & Poli, 1998; Syracuse et al., 2010; van Keken et al., 2011; Cerpa et al., 2022). Higher convergence rates, or the subduction of older lithosphere induce colder geothermal gradients in the downgoing plate in modern systems (Peacock et al., 1999; Syracuse et al., 2010).

Subduction zones with fast convergence of old oceanic lithosphere retain greater-water capacities at sub-arc depths (~30 mol.% H_2O: Fig. 3) compared to slower convergence of younger oceanic lithosphere (~4–15 mol.% H_2O: see also van Keken et al., 2011). Colder geothermal conditions enable retention of hydrous phases to deeper conditions (Schmidt & Poli, 1998; Grove et al., 2009; van Keken et al., 2011; Poli & Schmidt, 2014; Chapman et al., 2021). The *T*-sensitive dehydration reactions are inhibited, enabling phases like lawsonite, zoisite, phengite, chlorite, and antigorite to persist to greater depths (Fig. S1). In comparison, in warmer subduction geotherms these hydrous phases breakdown at shallower conditions (Poli & Schmidt, 2014).

During high slab flux events it is predicted 500–840±100 Tg km^{-2} Myr^{-1} of H_2O would be entering the sub-arc from the entire downgoing slab (Figs 1 & 3). The background amount of H_2O entering the sub-arc is less (40–200±30 Tg km^{-2} Myr^{-1}). The relative contributions to the H_2O budget from the lithospheric components during background subduction is mostly related to serpentinite (97–99%: chlorite and antigorite), less so basaltic

(~0.5–2%) and sediment (~0.5–1%) contributions (Fig. S2). In a high slab flux event, the contributions of basaltic (60–90%) and sedimentary (9–50%) sources increase drastically, with proportional less from serpentinite (0–40%) (Figs S2). Due to the colder and deeper subduction of the crustal components.

Progressive fluid release from the slab during subduction is known to hydrate or metasomatise the mantle wedge (Grove et al., 2009; Scambelluri et al., 2019). Hydration results in the production of serpentinite that will have a volume proportional to the fluid budget of the downgoing slab (Spandler & Pirard, 2015). Any displacement of hydrated portions of the mantle wedge or metasomatic rock to higher-*P* during the channel flow will provide additional H_2O release at sub-arc depths (Scambelluri et al., 2019). Although, the physical, chemical, and thermal behaviour of this portion of the subduction system remains poorly constrained and difficult to implement in the calculated budgets (Spandler et al., 2008; Spandler & Pirard, 2015).

3. Discussion

3.1. Deep time H_2O budgets and magmatism

The production of arc magma is dependent on the liberation of H_2O-rich fluid from the downgoing oceanic plate into the mantle wedge (Ringwood, 1974). Progressive release of fluid from the subducting plate occurs during its metamorphic transformation from blueschist to eclogite (Fig. S1: Schmidt & Poli, 2014; Chapman et al., 2019). Temporal increases in the volume of fluid entering zones of partial melting in the mantle wedge can thus drive the generation of greater volumes of magma (Ringwood, 1974; Grove et al., 2006). Increasing the amount of H_2O in the sub-arc permits proportionally greater melt production (upwards of 5 times) from that associated with a less hydrated peridotite (Schmidt & Poli, 1998; Cagnioncle et al., 2007; Grove et al., 2009).

The first order correlation between periods of greater slab flux and the volume of magmatism in the overriding plate supports a causal relationship (Fig. 1b). Changes in the volume and rate of subduction of oceanic lithosphere will have a direct bearing on the H_2O budget before accounting for other subduction variables. The thermal regime and angle of the subducting plate strongly influence the position of fluid liberation and thus capacity for related melting in the overlying mantle wedge (van Keken et al., 2011; Schmidt & Poli, 2014; Chapman et al., 2019). Higher convergence rates, and/or the subduction of older lithosphere, induce colder geothermal gradients in the downgoing plate and greater fluid liberation (mostly H_2O-rich) from blueschist and eclogite (Fig. 3: Clarke et al., 2006; Grove et al., 2009; Syracuse et al., 2010). Mantle wedge melting dynamics may also be compounded by variations in the distribution of heat in the wedge associated with changing angles of subduction (Gorczyk et al., 2007; Grove et al., 2009; England & Katz, 2010; Perrin et al., 2018).

To account for some of these additional factors the first time-dependent global estimate of H_2O budgets was established (Fig. 1d) by integrating predictions of H_2O-rich fluid proportions from phase equilibria modelling (Powell & Holland, 1988; Chapman & Clarke, 2021) with subduction volumes determined from plate reconstructions (Fig. 2) (Müller et al., 2016). The tectonic variables of oceanic crust age, lithospheric thickness, proportions of hydrated sediment, MORB and serpentinite, are directly related to rates of seafloor spreading (Merdith et al., 2019, 2020). Each of these variables influence the extent of hydration and alteration of the oceanic lithosphere. The effects of these variables have been incorporated into the global models of H_2O capacity, based on calculations of seafloor hydration over the last 150 million-years (Merdith et al., 2019).

The integration of these datasets suggests that during high subduction flux periods, there is a three- to five-fold increase in the H_2O released (500–840±100 Tg km^{-2} Myr^{-1}) into

289 the sub-arc relative to background subduction (40–200±30 Tg km^{-2} Myr^{-1}) (Fig. 1d). The
290 volume of subducted oceanic lithosphere, regardless of the thickness of sediment, controls
291 the magnitude of the H_2O available to drive magmatism (Fig. 2). The subduction flux is the
292 first order control, as similar variability in H_2O egress is apparent using other estimates of
293 fluid budgets (van Keken et al., 2011). Displacing the thermally controlled breakdown of
294 hydrous minerals to higher pressure conditions during high-convergence (>90 km Myr^{-1}) is
295 also influential (Schmidt & Poli, 2014; Chapman et al., 2019). In high-flux episodes the main
296 contributors (>50%) to H_2O budgets is oceanic crust and sediment. This equates to ~2–6
297 times the volume of H_2O released compared with low-flux periods (Fig. S2).

298 Subduction zone fluid budgets directly contribute to the volume of primitive arc melt
299 generated in the mantle wedge (Grove et al., 2009). Fluid ingress enables more fertile melting
300 of common peridotite sources (Cagnioncle et al., 2007). Flow dynamics of the mantle
301 continually introduce fertile (potentially fluid saturated) material into zones of partial melting
302 in the wedge (Gorczyk et al., 2007; England & Katz, 2010). The mobility of trace elements in
303 supercritical fluids or melts could contribute to enrichment of arc magmas or the
304 metasomatism the sub-arc mantle (Ringwood, 1974; Wyllie & Sekine, 1982; Kessel et al.,
305 2004; Hermann et al., 2006). These additional melt sources could contribute to greater melt
306 productivity during flare-up episodes.

307 *3.2. Magmatic pulses*

308 Higher resolution testing of how the subduction parameters influence flare-up volcanism can
309 be established by comparing results from individual arc margins (Fig. 3). During the *c*. 100–
310 130 Ma 'flare-up' in magmatic activity, increases in magma volumes of the main continental
311 arcs reached 100–1,000 times background levels (Ducea et al., 2007; DeCelles et al., 2009;
312 McKenzie et al., 2016; Milan et al., 2017). Pulses in magmatism recorded along the
313 Cretaceous portions of New Zealand and Antarctica show weak correlations to predicted

periods of high convergence, and episodes for the subduction of thick piles of sedimentary cover (Figs 3a & b). Instead, the flare-up magmatism at *c*. 100–130 Ma corresponds directly to an episode of increased slab flux and the related surge in H_2O egress (Figs 3a & b). A similar, though less pronounced association is apparent for volcanism at *c.* 150 Ma, plausibly linked to higher subducted sediment volumes that match records of accretionary metamorphism (Gray & Foster, 2004). The timing offset between peak slab flux and magmatic pulse is consistent with the lags inferred to be associated with descent rates of the subducting plate, and the timescales of magma and fluid egress (van Keken et al., 2011; Kirsch et al., 2016).

The coupled relationship between subduction flux and magmatic pulses can be observed along most of the circum-Pacific arcs in the Phanerozoic. The results of changing subduction flux can be tracked in the arc magmatic sections of South America (Patagonia) (Pepper et al., 2016) and north-eastern China–Korea–Japan (Tang et al., 2018). The volumetric magnitude of the magmatism during a pulses event is more difficult to estimate with respect to preservation biases in the magmatic record. Despite this, most prominent increases in subduction H_2O budgets are associated to spikes in magmatic activity through the circum-Pacific arcs (Fig. 3). Coupled episodes of metamorphism in the accretionary wedges and subsequent arc migration are also supported by predictions of periods of thicker sediment subduction. Such a causal relationship remains present in older (>150 Ma) magmatic events even though subduction flux predictions are more uncertain (Fig. 3). However, local-scale tectonic features on some margins makes comparative analysis on a global scale problematic. Delayed flare-up age relationships (*c*. 90–130 Ma) in North America are consistent with variability in global behaviour during the tectonic re-organization (Kirsch et al., 2016; Cao et al., 2017; Martínez Adrila et al., 2019). However, direct assessments of the slab flux are rendered difficult on account of assumptions regarding

local seafloor convergence that lacks paired isochrons in the North America region as well as disturbances from terrane docking (Kirsch et al., 2016; Martínez Adrila et al., 2019).

An external underlying tectonic control on magmatic pulse events does not preclude the operation of additional forcing mechanism associated with crustal processes in arcs (e.g. DeCelles et al., 2009; Ducea et al., 2015; Chapman et al., 2021). Triggering higher mantle fluxes at subduction zones aids in the redistribution of heat and the production of melts and fluids (Annen et al., 2006; DeCelles et al., 2009; Chapman et al., 2017; Chapman et al., 2021). Changes in heat flow regimes enable fertile crustal material to interact with mantle-derived liquids and produce additional volumes of magma via crustal anatexis. The processes can be accentuated by arc compression cycles or the lateral migration of magma pathways that enable fertile crustal material to interact with high-heat flow domains (DeCelles et al., 2009; Chapman et al., 2021). The cycles of arc compression or extension are linked to the rate and style of subduction convergence, though they vary along individual margins (Ducea et al., 2007; Kirsch et al., 2016). Predicted changes in subduction flux likely contribute to these magmatic migrations in arcs.

The intensification of advective heat-flow in arc crust is predicted to be associated with the influx of voluminous, hot, mantle-derived magma (Annen et al., 2006). Isotopic ratios (ε_{Hf} and $^{143}Nd/^{144}Nd$) of magmas from pulses in Cretaceous arcs across the global are consistent with the majority (80–90%) of the liquid source contribution being derived from the mantle wedge (Fig. 3: Kirsch et al., 2016; Milan et al., 2017; Martínez Adrila et al., 2019). The ratios support an underlying driver associated to changes in mantle melting dynamics. The evolution of isotopic ratios in arc magmas during a pulse event typically show a progressive crustal inheritance (lower ε_{Hf}) from the initial juvenile input (higher ε_{Hf}) (Fig. 3). The spread in isotopic inheritance from New Zealand, Antarctica and East Asia arcs is consistent with greater crustal interactions during prolonged high-heat magmatic flux,

associated to secondary melting processes in the arc crust (Fig. 3) (Milan et al., 2017; Tang et al., 2018). Similar dynamics are observed in other margins, where the volume contributions from crustal melts may be as large as 50% (e.g. Sierra Nevada) (Ducea & Burton, 2007; DeCelles et al., 2009; Chapman et al., 2021). There is no consistent correspondence in the generation of isotopically evolved magmas (low ε_{Hf}) and the subduction of thick piles of sediment (Fig. 3) (Herman et al., 2006; Ruscitto et al., 2012). This could relate to erosional effects during accretion and subsequent delays in dragging of sediment deep into the subduction system or limited isotopic influence in egressed fluids (Schmidt & Poli, 1998; Hermann et al., 2006; Clift & Vannucchi, 2004).

References

Annen, C. A., Blundy, J. D., Sparks, R. S. J. 2006. The genesis of intermediate and silcic magmas in deep crustal hot zones. *J. Petrol.*, **47**, 505–539.

Cagnioncle, A. M., Paramentier, E. M., Elkins-Tanton, L. T. 2007. Effect of solid flow above subducting slab on water distribution and melting at convergent plate boundaries. *J. Geophys. Res.*, **112**, B09402.

Campbell, I. H., Allen, C. M. 2008. Formation of supercontinents linked to increases in atmospheric oxygen. *Nature Geo.*, 1 doi: 10.1038/ngeo259.

Campbell, M. J., Rosenbaum, G., Allen, C., Spandler, C. 2020. Continental crustal growth processes revealed by detrital zircon petrochronology: insights from Zealandia. *J. Geophy. Res.: Solid Earth*, doi: 10.1029/2019JB019075.

Cao, W., Lee, C-T., Lackey, J. S. 2017. Episodic nature of continental arc activity since 750 Ma: a global compilation. *Earth Planet. Sci. Letts.*, **461**, 85–95.

Cerpa, N. G., Arcay, D., Padrón-Navarta, J. A. 2022. Sea-level stability over geological time owing to limited deep subduction of hydrated mantle. *Nature Geo*., doi: 10.1038/s41561-022-00924-3.

Chapman, T., Milan, L. A., Metcalfe, I., Blevin, P. L., Crowley J. 2022. Arc eruptions deliver 'first blow' in the pulsed end-Permian mass extinction. *Nature Geo.* **15**, 411–416.

Chapman, T., Clarke. G. L. 2021. Cryptic evidence for the former presence of lawsonite in blueschist and eclogite. *J, Metamorph. Geol.*, **39**, 343–362.

Chapman, T., Clarke, G. L., Dazcko, N. R. 2017. The role of buoyancy in the fate of ultra-high-pressure eclogite. *Sci. Reports.*, DOI: 10.1038/s41598-019-56475-y.

Chapman, T., Clarke, G. L., Piazolo, S., Daczko, N. R. 2019. Evaluating the importance of metamorphism in the foundering of continental crust. *Sci. Reports*, DOI:10.1038/s41598-017-13221-6.

Chapman, J. B., Shields, J. E., Ducea, M. N., Paterson, S. R., Attita, S., Ardill, K. E. 2021. The causes of continental arc flare-ups and drivers of episodic magmatic activity in Cordilleran orogenic systems. *Lithos*, 398–399, 106307.

Clarke, G. L., Powell, R., Fitzherbert, J. A. 2006. The lawsonite paradox: a comparison of field evidence and mineral equilibria modelling. *J. Metamorp. Geol.*, **24**, 715–725.

Clift, P., Vannucchi, P. 2004. Controls on tectonic accretion versus erosion in subduction zones: implications for the origin and recycling of the continental crust. *Rev. Geophy.,* 42, doi: 10.1029/2003RG000127.

Coulthard, D. A., Reagan, M. K., Shimizu, K., Bindeman, I. N., Brounce, M., Almeev, R., Ryan, J., Chapman, T., Shervais, J., Pearce, J. 2020. Magma source evolution following subduction initiation: evidence from the element concentrations, stable isotope ratios and water contents of volcanic glasses from the Bonin Forearc (IODP Expedition 352). *G^3,* doi: 10.1029/2020GC009054.

412 Davies, F. A., Tangeman, J. A., Tenner, T. J., Hirschmann, M. H. 2009. The composition of
413 KLB-1 peridotite. *Am. Mineral*. **94**, 176–180.
414 DeCelles, P. G., Ducea, M. N., Kapp, P., Zandt, G. 2009. Cyclicity in Cordilleran orogenic
415 systems. *Nature Geo.*, **2**, 251–257.
416 Domeier, M., Magni, V., Hounslow, M. W., Torsvik, T. H. 2018. Episodic zircon age spectra
417 mimic fluctuations in subduction. *Sci. Reports*, doi: 10.1038/s41598-018-35040-z.
418 Ducea, M. N., Barton, M. D. 2007. Igniting flare-up events in Cordilleran arcs. *Geology*, **35**,
419 1047–1050.
420 Ducea, M. N., Paterson, S. R., DeCelles, P. G. 2015. High-volume magmatic events in
421 subduction systems. *Elements*, **11**, 99–104.
422 East, M., Müller, R. D., Williams, S., Zahirovic, S., Heine, C. 2019. Subduction history
423 reveals Cretaceous slab superflux as a possible cause for the mid-Cretaceous plume
424 pulse and superswell event. *Gondwana Res.*, **79**, 125–139.
425 England, P. C., Katz, R. F. 2010. Melting above anhydrous solidus controls the location of
426 volcanic arcs. *Nature*, **467**, 700–703.
427 Evans, K. A., Bickle, M. J. 2005. An investigation of the relationship between bulk
428 composition, inferred reaction progress and fluid-flow parameters for layered
429 micaceous carbonates from Maine, USA. *J. Metamorph. Geol*., **23**, 181–197.
430 Evans, K. A., Powell, R. 2015. The effect of subduction on the sulphur, carbon, and redox
431 budget of lithospheric mantle. *J. Metamorph. Geol*. **33**. 649–670.
432 Faccenda, M. 2014. Water in the slab: a trilogy. *Tectonophysics*, **614**, 1–30.
433 Gorczyk, W., Willner, A. P., Gerya, T. V., Connelly, J. D., Burg, J-P. 2007. Physical controls
434 on magmatic productivity at Pacific-type convergent margins: numerical modelling.
435 *Phys. Earth Planet. Inter.*, **163**, 209–232.

436 Gray, D. R., Foster, D. A. 2004. $^{40}Ar/^{39}Ar$ thermochronologic constraints on deformation,
437 metamorphism and cooling/exhumation of a Mesozoic accretionary wedge, Otago
438 Schist, New Zealand. *Tectonophysics*, 385, 181–210.
439 Green, E. C. R., White, R. W., Diener, J. F. A., Powell, R., Holland, T. J. B., Palin, R. M.
440 2016. Activity–composition relations for the calculations of partial melting equilibria
441 for metabasic rocks. *J. Metamorph. Geol.* **34**, 845–869.
442 Grose, C. J. 2012. Properties of oceanic lithosphere: revised plate cooling model predictions.
443 *Earth Planet. Sci. Letts.*, **333**, 250–262.
444 Grove, T. L., Chatterjee, N., Parman, S. W., Médard, E. 2006. The influence of H_2O on
445 mantle wedge melting. *Earth Planet. Sci. Letts.*, **249**, 74–89.
446 Grove, T. L., Till, C. B., Lev, E., Chatterjee, N., Médard, E. 2009. Kinematic variables and
447 water transport control formation and location of arc volcanoes. *Nature*, **459**, 694–
448 697.
449 Hacker, B. 2008. H_2O subduction beyond arcs. G^3, doi:10.1029/2007GC001707.
450 Hawkesworth, C. J., Kemp, A. I. S. 2006. Evolution of the continental crust. *Nature*, doi:
451 10.1038/nature05191.
452 Hermann, J., Spandler, C., Hack, A., Korsakov, A. V. 2006. Aqueous fluids, and hydrous
453 melts in high-pressure and ultra-high-pressure rocks: implications for element transfer
454 in subduction zones. *Lithos*, **92**, 399–417.
455 Hermann, J., Spandler, C. 2008. Sediment melts at sub-arc depths: an experimental study. *J.*
456 *Petrol*., **49**, 717–740.
457 Holland, T. J. B., Powell, R. 2011. An improved and extended internally consistent
458 thermodynamic dataset for phases of petrological interest, involving a new equation
459 of state for solids. *J. Metamorph. Geol.* **29**, 333–383.

460 Holland, T. J. B., Powell, R. 2003. Activity–composition relations for phases in petrological
461 calculations: an asymmetric multicomponent formulation. *Cont. Mineral. Petrol* **145**,
462 492–501.
463 Iwasaki, I., Watanabe, T., Itaya, T., Yamazaki, M., Takigami, Y. 1995. Paleogene K–Ar ages
464 from Kamuikotan metamorphic rocks, southern area of the Kamuikotan Gorge,
465 central Hokkaido, northern Japan. *Geol. J.*, **30**, 281–295.
466 Jordan, T. A., Riley, T. R., Siddoway, C. S. 2019. The geological history and evolution of
467 West Antarctica. *Nature Reviews*, doi: 10.1058/s43017-019-00136.
468 Kessel, R., Schmidt, M. W., Ulmer, P., Pettke, T. 2004. Trace element signature of
469 subduction-zone fluids, melts, and supercritical liquids at 120–180 km depth. *Nature*,
470 **437**, 724–727.
471 Kirsch, M., Paterson, S. R., Wobbe, F., Martínez Adrila, A. M., Clauses, B., Alsino, P. H.
472 2016. Temporal histories of Cordilleran continental arcs: testing models for magmatic
473 episodicity. *Am. Mineral.*, **101**, 2133–2154.
474 Ma, Q., Xu, Y-G. 2021. Magmatic perspective on subduction of Paleo-Pacific plate and
475 initiation of big mantle wedge in East Asia. *Earth Sci. Rev.*, 213, 103473.
476 Martínez Adrila, A. M., Paterson, S. R., Memeti, V., Parada, M., Molina, P. G. 2019. Mantle-
477 driven Cretaceous flare-ups in Cordilleran arcs. *Lithos*, **326–327**, 19–27.
478 McKenzie, N. R., Horton, B. K., Loomis, S. E., Stockli, D. F., Planavsky, N. J., Lee C-T.
479 2016. Continental arc volcanism as the principal driver of icehouse-greenhouse
480 variability. *Science*, **352**, 444–447.
481 Merdith, A. S., Atkins, S. E., Tetley, M. G. 2019. tectonic controls on Carbon and
482 serpentinite storage in subducted upper oceanic lithosphere for the past 320 Ma.
483 *Front. Earth Sci.*, DOI: 10.3389/eart.2019.00332.

Merdith, A.S., del Real, P.G., Daniel, I., Andreani, M., Wright, N.M. and Coltice, N., 2020. Pulsated global hydrogen and methane flux at mid-ocean ridges driven by Pangea breakup. *Geochemistry, Geophysics, Geosystems*, 21(4), p.e2019GC008869

Milan, L. A., Daczko, N. R., Clarke, G. L. 2017. Cordillera Zealandia: A Mesozoic arc flare-up on the palaeo-Pacific Gondwana margin. *Sci. Reports*, DOI:10.1038/s41598-017-00347-w.

Müller, R. D., Seton, M., Zahirovic, S., Williams, S. E., Mathews, K. J., Wright, N. M., Shephard, G, E., Maloney, K. T., Barnett-Moore, N., Hosseinpour, M. 2016. Ocean basin evolution and global-scale plate reorganization events since Pangea breakup. *Annual Rev. Earth Planet. Sci.*, **44**, 107–138.

Nelson, D. A., Cottle, J. M. 2018. The secular development of accretionary orogens: linking the Gondwana magmatic arc record of West Antarctica, Australia, and South America. *Gond. Res.*, **63**, 15–33.

Osozawa, S., Usuki, T., Usuki, M., Wakabayashi, J., Jahn, B. 2019. Trace elemental and Sr–Nd–Hf isotopic compositions, and U–Pb ages for the Kitakami adakitic plutons: insights into interactions with the early Cretaceous TRT triple junction offshore Japan. *J. Asian Earth Sci.*, 184, 103968.

Palin, R. M., Weller, O. W., Waters, D. J., Dyck, B. 2016. Quantifying geological uncertainty in metamorphic phase equilibria modelling; a Monte Carlo assessment and implications for tectonic interpretations. *Geoscience Frontiers*, **7**, 591–607.

Palin, R. M., Santosh, M. 2021. Plate tectonics: what, where, why, and when? *Gond. Res.*, 100, 3–24.

Plank, T., Langmuir, C. H. 1998. The chemical composition of subducting sediment and its consequences for the crust and mantle. *Chem. Geol.,* 145, 325–394.

508 Pepper, M., Gehrels, G., Pullen, A., Ibanez-Mejia, M., Ward, K., Kapp, P. 2016. Magmatic
509 history and crustal genesis of western South America: Constraints from U–PB ages
510 and Hf isotopes of detrital zircons in modern rivers. *Geosphere*, 12, 1–24.
511 Powell, R., Holland, T. J. B. 1988. An internally consistent dataset with uncertainties and
512 correlations: 3. Applications to geobarometry, worked examples and a computer
513 program. *J. Metamorph. Geol.* **6**, 173–204.
514 Powell, R., Holland, T. J. B. 2008. On thermobarometry. *J. Metamorph. Geol.*, **26**, 155–176.
515 Ringwood, A. E. 1974. The petrological evolution of island arc systems. *J. Geol. Soc.*
516 *London*, **130**, 183–204.
517 Ruscitto, D. M., Wallace, P., Cooper, L. B., Plank, T. 2012. Global variation in H_2O/Ce 2.
518 Relationships to arc magma geochemistry and volatile fluxes. G^3, **Q03025**.
519 Spandler, C., Hermann, J., Faure, K., Mavrogenes, J. A., Arculus, R. 2008. The importance
520 of talc and chlorite "hybrid" rocks for volatile recycling through subduction zones;
521 evidence from the high-pressure subduction mélange of New Caledonia. *Contrib.*
522 *Mineral. Petrol.*, **155**, 181–198.
523 Spandler, C., Pirard, C. 2015. Element recycling from subducted slabs to crust: a review.
524 *Lithos*, **170–171**, 208–223.
525 Schmidt, M. W., Poli, S. 1998. Experimentally based water budgets for dehydrating slabs and
526 consequences for arc magma generation. *Earth Planet. Sci. Lett.*, **163**, 361–
527 379.Schmidt, M. W., Poli, S. 2014. Devolatilization during subduction. In. Rudnick
528 (Ed.) *Treatise in Geochemistry*, Elsevier, Amsterdam. 669–701.
529 Syracuse, E. M., van Keken, P. E., Abers, G. A. 2010. The global range of subduction zone
530 thermal models. *Phys. Earth Planet. Interiors*. **183**, 73–90.

Tang, J., Xu, W., Wang, F., Ge, W. 2018. Subduction history of the Paleo-Pacific slab beneath Eurasian continent: Mesozoic–Paleogene magmatic records in Northeast Asia. *China Earth Sci*, **61**, 527–559.

Till, C. B., Kent, A. J. R., Abers, G. A., Janiszewski, H. A., Gaherty, J. B., Pitcher, B. W. 2021. The causes of spatiotemporal variations in erupted fluxes and compositions along a volcanic arc. *Nature Comm.,* doi: 10.1038/s41467-019-09113-0.

van Keken, P. E., Hacker, B. R., Syracuse, E. M., Abers, G. A. 2011. Subduction factory 4: depth dependent flux of H_2O from subducting slabs worldwide. *J. Geophys. Res., **116,*** B01401**.**

Voice, P. I., Kowalewski, M., Eriksson, K. A. 2011. Quantifying the timing and rate of crustal evolution: global compilation of radiometrically dated detrital zircon grains. *J. Geology*, 119, 109–126.

White, R. W., Powell, R., Holland, T. J. B., Johnson, T. E., Green, E. C. R. 2014. New mineral activity–composition relations for thermodynamic calculations in metapelitic systems. *J. Metamorph. Geol.* **32**, 261–286.

Wyllie, P. J., Sekine, T. 1982. The formation of mantle phlogopite in subduction zone hybridization. *Contrib. Mineral. Petrol.*, **79**, 375–380.

Zahirovic, S., Eleish, A., Doss, S., Pall, J., Cannon, J., Pistone, M., Fox, P. 2022. Subduction and carbonate platform interactions. *Geos. Data J.* **00**, 1–13.

Captions

Figure 1 Global distribution of U–Pb zircon crystallisation ages representative of episodic magmatic activity in relation to supercontinent cycles (amber bars) (Voice et al., 2011). (a) Average convergence rates for global subduction zones over the last 230 million years. (b) Calculated slab flux volumes over the last 500 million-years. Solid lines represent high-

confidence data established from plate reconstructions in the last 200 Ma and dotted lines are projections based on longer term plate velocities after Domeier et al. (2018). (c) Predictions of the average subducted sediment volume over the last 200 million years. (d) Calculation of the time-dependent fluid flux entering sub-arcs (shadow encompasses uncertainties), including estimates using H_2O input values of van Keken et al. (2011) (green).

Figure 2 Global tectonic plate reconstruction at c. 120 Ma showing arc convergence rates and age of the oceanic crust.

Figure 3 Comparison of H_2O flux (top–line thickness encompasses uncertainties), subducted sediment thickness (middle) and (bottom) εHf isotope relations against zircon age distribution on (a) the New Zealand–Antarctica margin from c. 75–200 Ma (Nelson & Cottle, 2018; Campbell et al., 2020). (b) the Antarctica–Patagonia margin from c. 75–200 Ma (Ducea et al., 2015; Pepper et al., 2016; Nelson & Cottle, 2018; Jordan et al., 2019;) and (c) the East Asia (northern China, Korea, and Japan) margin from c. 75–200 Ma (Iwasaki et al., 1995; Tang et al., 2018; Osozawa et al., 2019; Ma & Xu, 2021).

Acknowledgments: We appreciate helpful guidance on the specifics of some THERMOCALC calculations provided by R. Powell, E. Green, and K. Evans. T. C. and L. A. M. were supported via funding through the School of Environment and Rural Sciences at University of New England. A. M. received funding from Marie Curie Fellowship NEOEARTH, project 893615. G. L. C. received funding from the Faculty of Science at the University of Sydney. S. Z. was supported by Australian Research Council grant DE210100084 and a University of Sydney Robinson Fellowship. GPlates and pyGPlates development is funded by the AuScope National Collaborative Research Infrastructure System (NCRIS) program. N. D. was supported by Australian Research Council grant DP200100482. We thank for R. Palin for helpful comments during revision.

Data Availability Statement: The data supporting this study can be found in the supporting information and at the website https://osf.io/zxuwa/?view_only=b04200e1bf214612b70b4d90015cab1f with DOI: https://doi.org/10.17605/OSF.IO/ZXUWA. The GPlates reconstruction models (Global rotation model, dynamic polygons, spreading ridge and isochron files) are available at https://www.earthbyte.org/gplates-2-3-software-and-data-sets/. Thermodynamic data used in the study is available in the reference Holland & Powell (2011). *(https://doi.org/10.1111/j.1525-1314.2010.00923.x)*.

Figure 1.

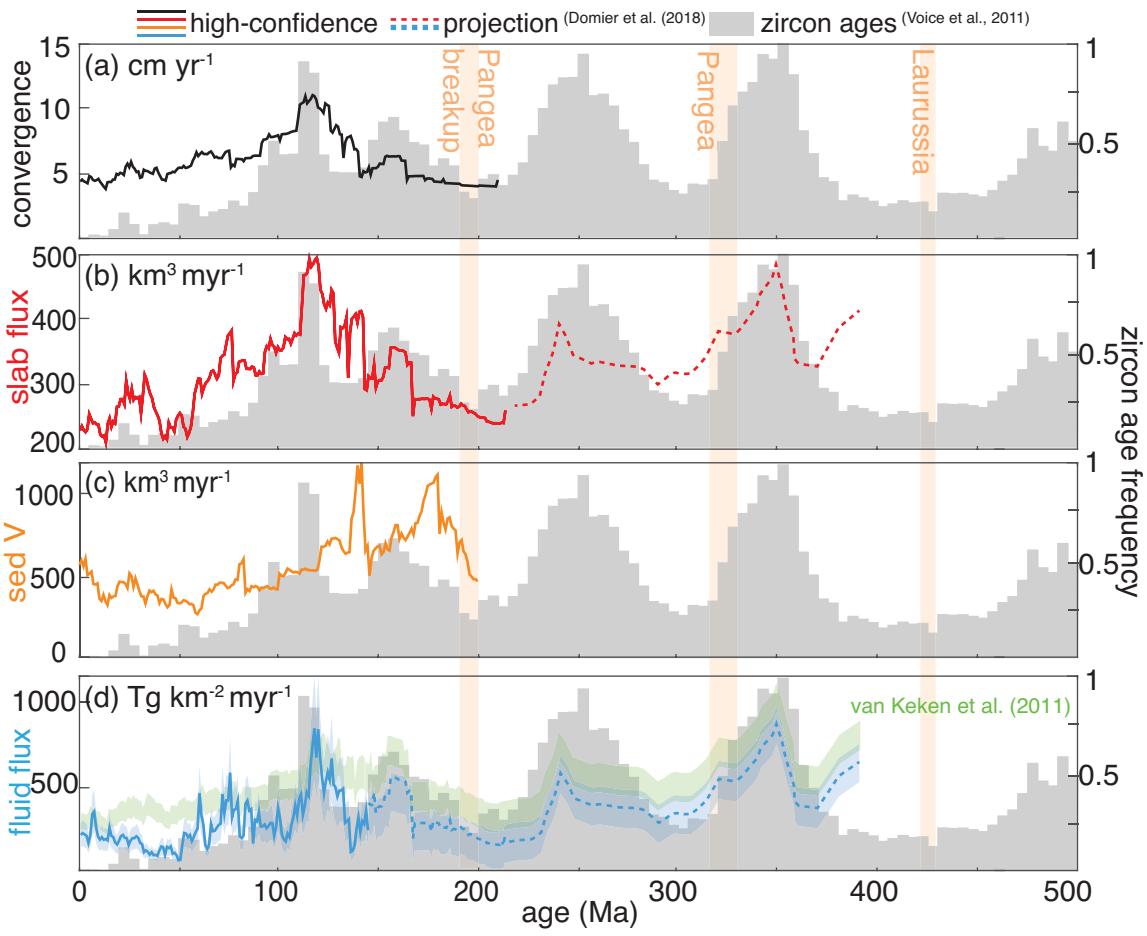
high-confidence
projection (Domier et al. (2018)
zircon ages (Voice et al., 2011)
(a) cm yr-1
convergence
Pangea breakup
Pangea
Laurussia
(b) km3 myr-1
slab flux
(c) km3 myr-1
sed V
(d) Tg km-2 myr-1
fluid flux
van Keken et al. (2011)
zircon age frequency
age (Ma)

Figure 2.

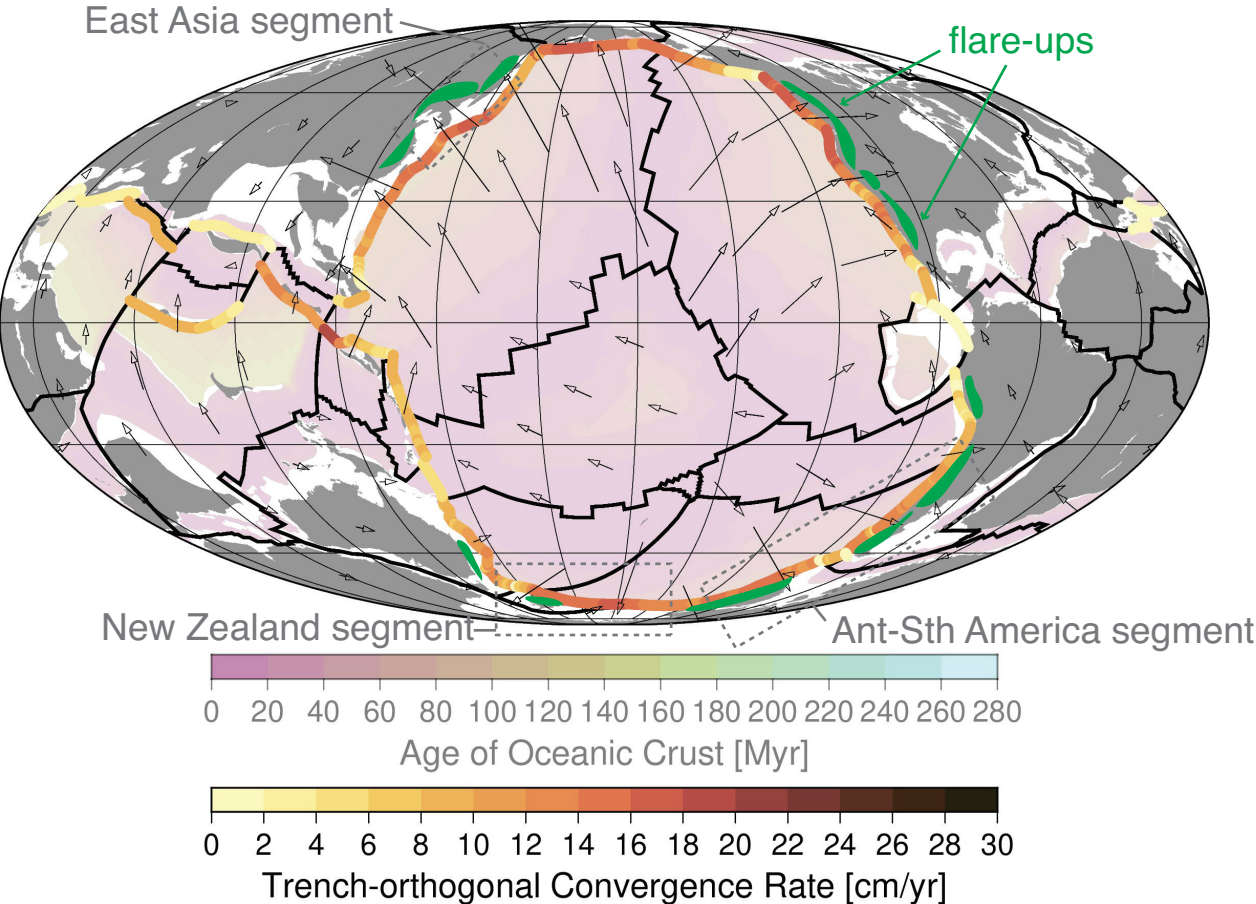
East Asia segment
flare-ups
New Zealand segment
Ant-Sth America segment
0 20 40 60 80 100 120 140 160 180 200 220 240 260 280
Age of Oceanic Crust [Myr]
0 2 4 6 8 10 12 14 16 18 20 22 24 26 28 30
Trench-orthogonal Convergence Rate [cm/yr]

Figure 3.

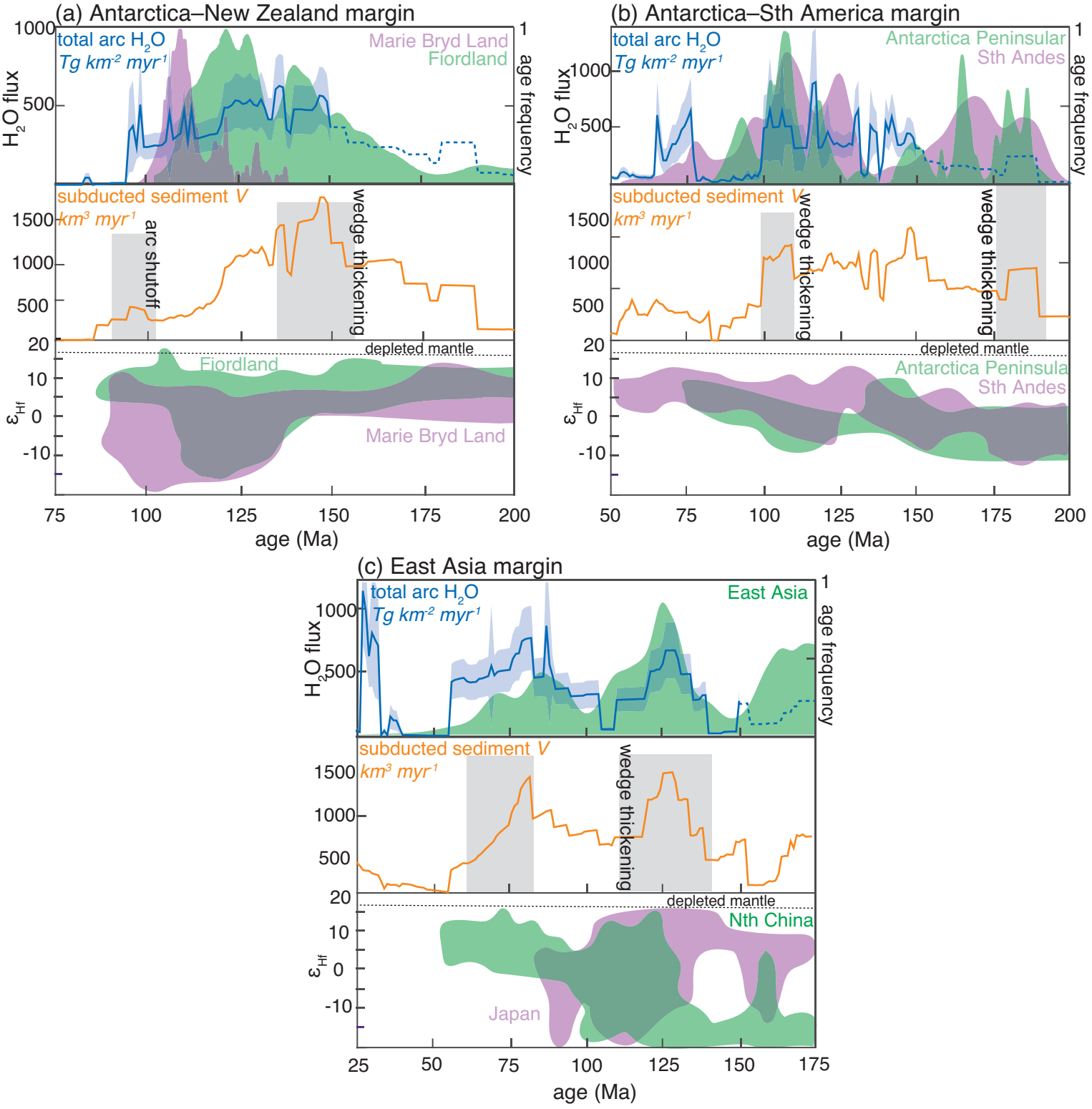
(a) Antarctica–New Zealand margin
total arc H2O
Tg km-2 myr-1
Marie Bryd Land
Fiordland
H2O flux
age frequency
subducted sediment V
km3 myr-1
arc shutoff
wedge thickening
depleted mantle
Fiordland
Marie Bryd Land
εHf
age (Ma)
(b) Antarctica–Sth America margin
total arc H2O
Tg km-2 myr-1
Antarctica Peninsular
Sth Andes
subducted sediment V
km3 myr-1
wedge thickening
wedge thickening
depleted mantle
Antarctica Peninsula
Sth Andes
age (Ma)
(c) East Asia margin
total arc H2O
Tg km-2 myr-1
East Asia
subducted sediment V
km3 myr-1
wedge thickening
depleted mantle
Nth China
Japan
age (Ma)